Evanescent waves of an annular left-handed material lens

Changchun Yan (闫长春)[1,2], Yiping Cui (崔一平)[1*], Qiong Wang (王 琼)[1], and Changgui Lü (吕昌贵)[1]

[1] *Advanced Photonics Center, School of Electronic Science and Engineering, Southeast University, Nanjing 210096*

[2] *School of Physics and Electronic Engineering, Xuzhou Normal University, Xuzhou 221116*

[*] *E-mail: cyp@seu.edu.cn*

Received September 16, 2008

The imaging system formed by an annular left-handed material (LHM) lens as well as the evanescent waves in the lens are simulated numerically with a finite-difference time-domain (FDTD) method. For $b-a>\lambda$ (a and b are respectively the inner and outer radii of the annular lens, and λ is the wavelength), when a point source is placed at an internal grid point, we demonstrate that the evanescent waves are produced around the internal interface, and cannot propagate outwards. As for $b-a<\lambda$, the evanescent waves appear around both the internal and the external interfaces, which remarkably implies the coupling between the two interfaces. Hence it can be inferred that the evanescent waves around the external interface participating in the super-resolution imaging result from the coupling of the evanescent waves around the interface. Moreover, the partly uncomprehended properties of the evanescent waves in the LHM slab are also disclosed. It is conducive to understanding the evanescent waves in the LHMs further.

OCIS codes: 160.4760, 260.5740, 100.6640.

doi: 10.3788/COL20090702.0134.

It has been nearly 40 years since Veselago proposed that the combination of negative permittivity ($\varepsilon<0$) and negative permeability ($\mu<0$) leads to a negative refractive index[1]. However, the first demonstration of left-handed materials (LHMs) was in 2000[2], which causes increasing interests of researchers. At present, great progress has been made in producing the LHMs[3−11]. The extreme attention to the LHMs results from their unique properties and potential applications, such as reversal of both the Doppler shift and Cherenkov radiation[1,12], negative refraction[13], imaging of superlens[14−17], enhanced nonlinearity[18], specific field distribution of guided modes[19], etc. Undoubtedly, one of the important properties of the LHMs is the amplification of evanescent waves[20,21]. This amplification leads to the super-resolution imaging in the near fields[16,17,22,23]. In the past, the researchers more examined the evanescent waves of a LHM planar lens[14,22,24−26]. Although Pendry *et al.* ever discussed about the annular LHM lens, they paid attention to its perfect imaging but less studied its evanescent waves[27,28].

In this letter, the full-wave imaging of an annular LHM lens is simulated with a finite-difference time-domain (FDTD) method. The evanescent fields around the interfaces of the lens are investigated. The simulations and analyses show some characteristics of the evanescent waves in the annular lens. It is conducive to understanding the evanescent waves in the LHMs further. Meanwhile, from these characteristics, we can infer that the coupling of the evanescent waves results in the super-resolution imaging.

The two-dimensional (2D) imaging system we consider here contains an annular LHM lens, which is surrounded by vacuum, with an internal radius a and an external radius b (see Fig. 1). Following the description in Ref. [28], the annular lens can produce a magnified image of an internal object, and a demagnified image of an external object. Namely, the object closer than $r=b^2/a$ can form a demagnified image inside the annulus. Conversely, the objects within the annulus and farther than $r=a^2/b$ to the center will produce a magnified image outside the annulus. This statement will be verified below. We assume 2D transverse electric fields in a cylindrical coordinate system (E_z, H_θ, $H_r\neq 0$). The lens is supposed to be isotropic and characterized by relative permittivity and permeability of identical plasmonic form as[29,30]

$$\varepsilon_{\rm r}(\omega)=\mu_{\rm r}(\omega)=1-\frac{\omega_{\rm p}^2}{\omega^2-{\rm i}\omega\tau}, \tag{1}$$

where $\omega_{\rm p}$ is the plasma frequency and τ is the collision frequency. Emphatically, although the isotropic medium is assumed in our simulations, the simulation results below are similar to those for the anisotropic medium in Ref. [28]. In addition, a point source is expressed as $E_z(r,\theta,t)=E_z(r,0,t)=\sin(\omega t)$. Choosing $\omega=1.885\times10^{11}$ rad/s, $\omega_{\rm p}=2.6658\times10^{11}$ rad/s, and $\tau=1.885\times10^{8}$ rad/s, we can obtain $\varepsilon_{\rm r}(\omega)=\mu_{\rm r}(\omega)=-1-{\rm i}\gamma=-1.0-0.002{\rm i}$ (refractive index $n=-1.0-0.002{\rm i}$). Obviously, the annular lens is a matched and loss material. We employ the FDTD method and a perfectly matched layer (PML) boundary condition in the cylindrical coordinate system[31] to simulate the electromagnetic fields. A spatial step of $\Delta r=\lambda/30$, an angle step of $\Delta\theta=2\pi/300$, a time step of

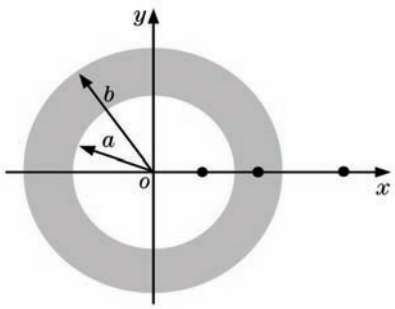

Fig. 1. Schematic of an annular HLM lens with marks.

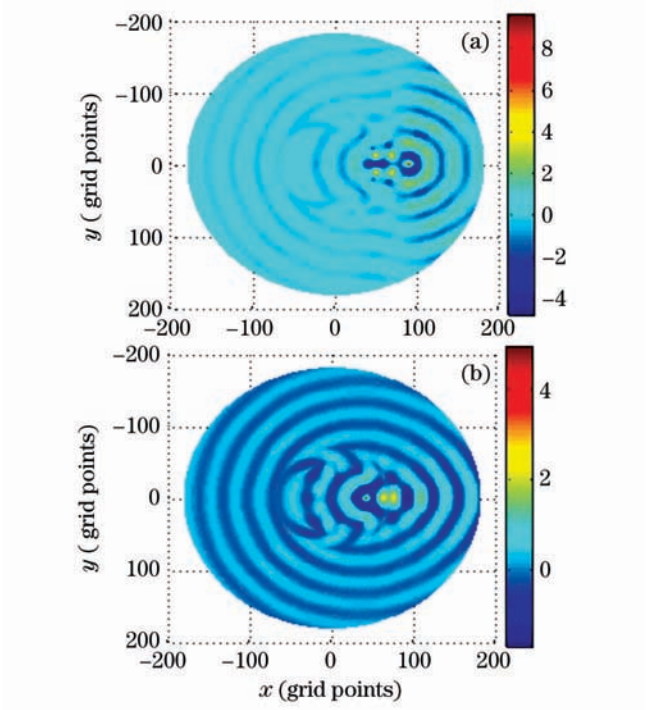

Fig. 2. (a) Snapshot of the electric field at time $20T_0$, the source point is placed at an external grid point (90,1); (b) snapshot of the electric field at time $13T_0$, the source point is placed at an internal grid point (42,1).

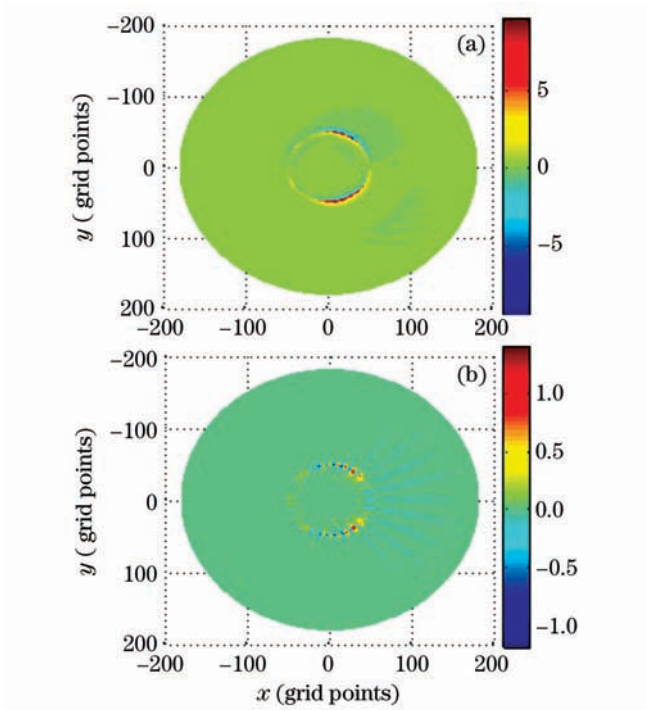

Fig. 3. Time-averaged energy streams (a) $\mathbf{S}_\theta$ and (b) $\mathbf{S}_r$ in the θ and r directions. The source has been turned on for $20T_0$ and thereafter turned off for $100T_0$. The source point is placed at an internal grid point (47,1), and the thickness of the annular lens equals $5/3\lambda$.

$\Delta t = \Delta r/(50c)$, and a primary computational domain 180 by 300 cells are applied in our simulations. Here the wavelength λ equals cT_0, T_0 is a period of the point source, and c is the velocity of light in free space. The annular lens occupies 20 by 300 cells ($a = 49\Delta r$ and $b = 70\Delta r$). If the source point is placed at an external grid point (90,1) ($r = 89\Delta r$, $\theta = 0$), the snapshot of the simulated electric fields at time $20T_0$ is shown in Fig. 2(a). From this figure, we can see that two focusing images appear respectively in the annular lens and in the internal region. Figure 2(b) represents the snapshot at time $13T_0$, when the point source is set at an internal grid point (42,1) ($r = 41\Delta r$, $\theta = 0$). Evidently, two amplified images are also formed. Hence our simulation results are in agreement with the description in Ref. [28]. In our simulations, we find that the images oscillate over time, as is similar to the images using LHM slabs[32]. This phenomenon results from a beating effect involving a vortex-like surface wave[33−35]. However, the image in the external region hardly oscillates. The reason is that this image is far from the annular lens (larger than λ). Thus the surface waves almost do not contribute to the image.

Now we consider the case of $b - a > \lambda$. To investigate the evanescent fields around the annular lens, the point source must be switched off for enough time. The intention is to make all propagating waves leave. Additionally, an angle step of $\Delta\theta = 2\pi/260$ and a primary computational domain 180 by 260 cells are employed. We suppose $a = 49\Delta r$ and $b = 99\Delta r$ ($b-a = 5\lambda/3$). The point source is placed at an internal grid point (47,1). Note that the source is away from the center, which can produce the evanescent waves around the interfaces of the annular lens. After the source has been turned on for $20T_0$ and thereafter turned off for $100T_0$, the distributions of energy streams $\mathbf{S}_\theta$ and $\mathbf{S}_r$ are displayed in Fig. 3, where $\mathbf{S}_\theta$ and $\mathbf{S}_r$ denote the average energy stream in the θ and r directions, respectively. From Figs. 3(a) and (b), we can see that the energy of the evanescent waves is only converged around the internal surface. This converged energy, consisting of energy-stream loops as revealed in Ref. [25], is so-called standing waves. The propagating waves marching into the internal surface are still the propagating waves on the external surface following the simulation results and analyses. As a result, evanescent waves cannot be produced around the external surface, and the evanescent waves are amplified merely in the thin layer of the lens. For an infinite-size LHM slab, in front of which a point source is placed, we can infer that the evanescent waves are engendered and magnified just around the front surface, when the thickness of the slab is longer than wavelength. Therefore, for a finite-size LHM slab, the evanescent waves of the back interface should merely result from the diffraction of those of the front interface through the side ends and the corners.

If the point source is laid at an external grid point (150,1) and other conditions are the same as those in Fig. 3, the $\mathbf{S}_\theta$ distributions of evanescent fields are shown in Fig. 4. Obviously, the evanescent waves occur not only around the external interface but also around the internal interface. This indicates that the evanescent waves around the internal surface originate from a part of propagating waves transmitting through the external surface.

Now we will examine the evanescent fields around the annular lens when its thickness is shorter than a wavelength, that is, the case of $b - a < \lambda$. Thus we assume $\Delta r = \lambda/100$, $a = 49\Delta r$, and $b = 69\Delta r$ (i.e., the thickness

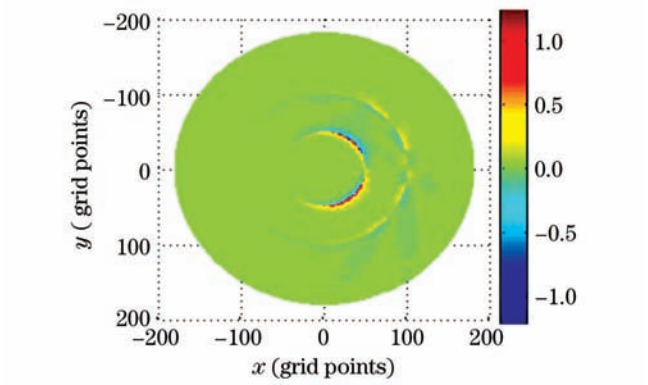

Fig. 4. Time-averaged energy stream $\mathbf{S}_\theta$ in the θ direction after the source has been turned on for $20T_0$ and thereafter turned off for $100T_0$. The point source is placed at an external grid point (150,1), and the thickness of the annular lens equals $5/3\lambda$.

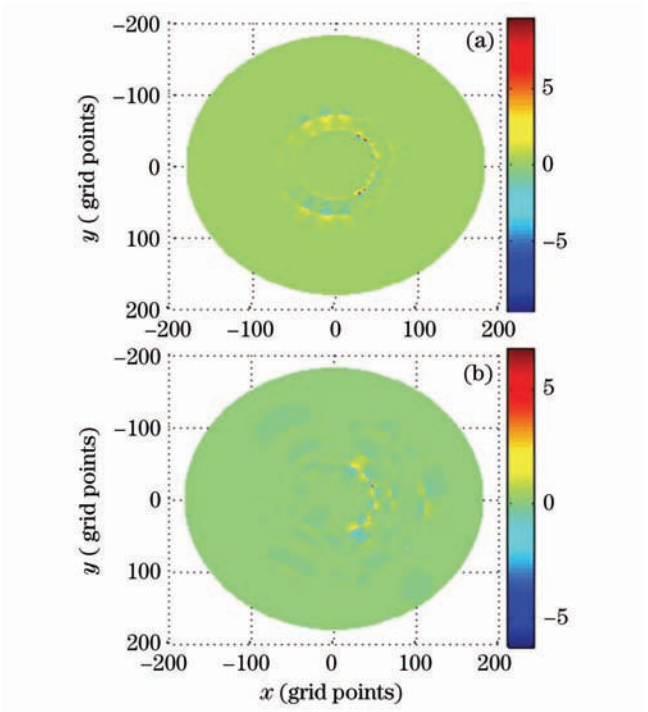

Fig. 5. (a) Time-averaged energy stream $\mathbf{S}_\theta$ of one annular lens after the source has been turned on for $6T_0$ and thereafter turned off for $30T_0$. The point source is placed at an internal grid point (47,1), and the thickness of the annular lens equals 0.2λ. (b) Time-averaged energy stream $\mathbf{S}_\theta$ of two annular lenses after the source has been turned on for $3T_0$ and thereafter turned off for $15T_0$. The point source is placed at an internal grid point (47,1), and both the thickness of every annular lens and the distance between them equal 0.1λ.

equals 0.2λ). The other conditions are the same as those in Fig. 3. After the source has been switched on for $6T_0$ and thereafter switched off for $30T_0$, the simulation results are shown in Fig. 5(a). From this figure, we can see that the evanescent waves still appear around the external interface, which is remarkably different from the case in Fig. 3(a). This implies that the coupling occurs between the two interfaces. Consequently, the evanescent waves around the external interface participating in the super-resolution imaging result from the coupling of the evanescent waves around the interface. For a finite-size LHM slab with a point source placed in front of it, we can infer that the evanescent waves can be diffracted near the side ends and the corners, and also coupled directly between the two slab surfaces, when the thickness of the slab is shorter than a wavelength.

Below, we assume that there is another same-center annular lens. Its internal and external radii are respectively set as $a' = 89\Delta r$ and $b' = 109\Delta r$. The spatial step is $\Delta r = \lambda/200$. The other conditions are like those in Fig. 5(a). Evidently, both the thickness of every annular lens and the distance between them are equal to 0.1λ. After the source has been turned on for $3T_0$ and thereafter turned off for $15T_0$, the evanescent fields are shown in Fig. 5(b). The simulation results verify that the coupling occurs between any neighboring surfaces.

For $b-a \sim \lambda$, our additional simulations show that the coupling between the two surfaces is greatly weak.

In conclusion, the imaging system constructed by an annular LHM lens has been simulated with the FDTD method. The properties of the evanescent waves in this lens have also been studied. For $b-a > \lambda$, when the point source is placed at the internal grid point, we demonstrate that the evanescent waves are produced around the internal interface and amplified merely in the thin layer of the lens. It is inferred that, for the infinite-size LHM slab, in front of which a point source is placed, the evanescent waves are engendered and magnified just around the front surface. For a finite-size LHM slab, the evanescent waves around the back interface result from the diffraction of those of the front interface through the side ends and the corners. As far as $b-a < \lambda$ is concerned, when the point source is still laid at the internal grid point, the evanescent waves also appear around the external interface, which indicates that the coupling occurs between the two interfaces. Consequently, the evanescent waves around the external interface participating in the super-resolution imaging result from the coupling of the evanescent waves around the interface. For a LHM slab, the evanescent waves can be coupled directly between the two surfaces of the slab. Moreover, as for $b-a \sim \lambda$, the coupling between the two interfaces is greatly weak.

References

1. V. G. Veselago, Sov. Phys. Uspekhi **10,** 509 (1968).
2. D. R. Smith, W. J. Padilla, D. C. Vier, S. C. Nemat-Nasser, and S. Schultz, Phys. Rev. Lett. **84,** 4184 (2000).
3. R. A. Shelby, D. R. Smith, and S. Schultz, Science **292,** 77 (2001).
4. T. J. Yen, W. J. Padilla, N. Fang, D. C. Vier, D. R. Smith, J. B. Pendry, D. N. Basov, and X. Zhang, Science **303,** 1494 (2004).
5. S. Linden, C. Enkrich, M. Wegener, J. Zhou, T. Koschny, and C. M. Soukoulis, Science **306,** 1351 (2004).
6. S. Zhang, W. Fan, B. K. Minhas, A. Frauenglass, K. J. Malloy, and S. R. J. Brueck, Phys. Rev. Lett. **94,** 037402 (2005).
7. S. Zhang, W. Fan, N. C. Panoiu, K. M. Malloy, R. M. Osgood, and S. R. J. Brueck, Phys. Rev. Lett. **95,** 137404 (2005).
8. G. Dolling, C. Enkrich, M. Wegener, C. M. Soukoulis, and S. Linden, Science **312,** 892 (2006).

9. G. Dolling, M. Wegener, C. M. Soukoulis, and S. Linden, Opt. Lett. **32,** 53 (2007).
10. H. J. Lezec, J. A. Dionne, and H. A. Atwater, Science **316,** 430 (2007).
11. H. Zhang, Y. Niu, S. Jin, R. Li, and S. Gong, Chin. Opt. Lett. **5,** S222 (2007).
12. A. Grbic and G. V. Eleftheriades, J. Appl. Phys. **92,** 5930 (2002).
13. D. R. Smith and D. Schurig, Phys. Rev. Lett. **90,** 077405 (2003).
14. J. B. Pendry, Phys. Rev. Lett. **85,** 3966 (2000).
15. N. Fang and X. Zhang, Appl. Phys. Lett. **82,** 161 (2003).
16. L. Zhao and T. J. Cui, Appl. Phys. Lett. **89,** 141904 (2006).
17. V. A. Podolskiy and E. E. Narimanov, Opt. Lett. **30,** 75 (2005).
18. H. Zhang, Y. Niu, H. Sun, and S. Gong, Chin. Opt. Lett. **6,** 373 (2008).
19. Z. Wang, J. Zhou, L. Zhang, H. Ren, and C. Jin, Acta Opt. Sin. (in Chinese) **28,** 1558 (2008).
20. Z. Liu, N. Fang, T.-J. Yen, and X. Zhang, Appl. Phys. Lett. **83,** 5184 (2003).
21. T. J. Cui, X. Q. Lin, Q. Cheng, H. F. Ma, and X. M. Yang, Phys. Rev. B **73,** 245119 (2006).
22. N. Garcia and M. Nieto-Vesperinas, Phys. Rev. Lett. **88,** 207403 (2002).
23. K. Aydin, I. Bulu, and E. Ozbay, Appl. Phys. Lett. **90,** 254102 (2007).
24. X. S. Rao and C. K. Ong, Phys. Rev. B **68,** 113103 (2003).
25. C. Liu, C. Yan, H. Chen, Y. Liu, and S. Gao, Appl. Phys. Lett. **88,** 231102 (2006).
26. L. Chen, S. He, and L. Shen, Phys. Rev. Lett. **92,** 107404 (2004).
27. J. B. Pendry and S. A. Ramakrishna, J. Phys. Condens. Matter **14,** 8463 (2002).
28. J. B. Pendry, Opt. Express **11,** 755 (2003).
29. J. B. Pendry, A. J. Holden, W. J. Stewart, and I. Youngs, Phys. Rev. Lett. **76,** 4773 (1996).
30. S. A. Cummer, Appl. Phys. Lett. **82,** 1503 (2003).
31. H. Zhang, Y. Lü, and P. He, J. Microwaves (in Chinese) **20,** (3) 19 (2004).
32. X. S. Rao and C. K. Ong, Phys. Rev. E **68,** 067601 (2003).
33. L. Zhou and C. T. Chan, Appl. Phys. Lett. **86,** 101104 (2005).
34. L. Zhou and C. T. Chan, Opt. Lett. **30,** 1812 (2005).
35. X. Huang, L. Zhou, and C. T. Chan, Phys. Rev. B **74,** 045123 (2006).